ADVANCING EARTH AND SPACE SCIENCES

Geophysical Research Letters

RESEARCH LETTER
10.1029/2025GL120583

Special Collection:
Land-atmosphere coupling: measurement, modelling and analysis

Unlocking Urban Climate Change Analysis in Global Kilometer-Scale Climate Simulations

Xabier Pedruzo-Bagazgoitia[1], Birgit Sützl[1], Emanuel Dutra[2], Joe McNorton[3], Aristofanis Tsiringakis[1], and Christoph Rüdiger[1]

[1]European Centre for Medium-Range Weather Forecasts (ECMWF), Bonn, Germany, [2]Instituto Português do Mar e da Atmosfera (IPMA), Lisbon, Portugal, [3]European Centre for Medium-Range Weather Forecasts (ECMWF), Reading, UK

Key Points:

- We validate globally, at hourly and down to 4 km resolution, a method to define rural and urban areas in km-scale climate simulations
- Beyond city-specific results, simulations suggest a mean accelerated warming of rural areas, resulting in future weaker urban heat island effects
- Km-scale climate simulations open new possibilities, allowing new questions, in the science of urban climate

Supporting Information:

Supporting Information may be found in the online version of this article.

Correspondence to:

X. Pedruzo-Bagazgoitia,
xabier.pedruzo@ecmwf.int

Citation:

Pedruzo-Bagazgoitia, X., Sützl, B., Dutra, E., McNorton, J., Tsiringakis, A., & Rüdiger, C. (2026). Unlocking urban climate change analysis in global kilometer-scale climate simulations. *Geophysical Research Letters*, *53*, e2025GL120583. https://doi.org/10.1029/2025GL120583

Received 25 NOV 2025
Accepted 21 APR 2026

Author Contributions:

Conceptualization: Xabier Pedruzo-Bagazgoitia, Birgit Sützl
Data curation: Xabier Pedruzo-Bagazgoitia, Birgit Sützl, Emanuel Dutra
Formal analysis: Xabier Pedruzo-Bagazgoitia, Birgit Sützl, Aristofanis Tsiringakis
Investigation: Xabier Pedruzo-Bagazgoitia, Birgit Sützl, Joe McNorton, Aristofanis Tsiringakis

Abstract Coupled multi-decadal global km-scale simulations completed in recent years open new perspectives in the investigation and understanding of urban climate change. This study introduces a generic method for extracting urban areas and their rural references worldwide and validates it on hourly timescales with remote-sensing observations of land-surface temperature for over 400 cities, while identifying the key role of spatial resolution. We showcase the immense amount of hourly data available for each city for 60 years of past and future climate in the Next Generation Earth Modelling Systems simulations, and how these simulations represent surface-atmosphere interactions driven by urban areas. We finally propose city clustering as a method to exploit these simulations and move beyond city-specific results. Results suggest a mean potential decrease in future urban heat island intensity driven by stronger rural warming for all clusters except for cold climates.

Plain Language Summary Current methods to investigate how climate change affect cities have several limitations. New very high-resolution (10 km or finer) climate simulations allow to overcome many of those limitations. First, we propose a method to identify urban areas worldwide, and to set up a rural reference for each of them to better understand the particular climate effects over cities. We use and validate with satellite observations the method over more than 400 cities for model simulations with increasing spatial resolution, and find the very high resolution is needed to represent the temperature effects of cities. We also show very high resolution simulations from the Next Generation Earth Modelling Systems project and how much information, both in time and in space, they contain with respect to cities on a changing climate. Finally, we also try to aggregate cities according to city characteristics such as their climate (tropical, cold, arid or temperate), to infer more general city behavior on a changing climate. Very high resolution simulations of future climate suggest that rural areas warm up faster than the cities nearby, and therefore the typical effect of cities being warmer than their surroundings weakens.

1. Introduction

With a constantly increasing share of the world's population living in cities, and the threat of climate change, it is of critical relevance to provide studies that inform both technical and broad audiences on the urban-specific climate risks. The state-of-the-art analysis for future urban climate relies on four alternative approaches: (a) statistical or dynamic downscaling of climate simulations as proposed by the CORDEX initiative and others (Duchêne et al., 2020; Langendijk et al., 2024), (b) global uncoupled surface modeling lacking surface-atmosphere feedbacks (Lauwaet et al., 2015), (c) city or region-specific case studies using local modeling or machine learning methodologies for current or future climates (Johannsen et al., 2024; Lemonsu et al., 2013; Zhao et al., 2014), and (d) the use of urban scheme emulators to obtain urban information from global low-resolution climate simulations (Zhao et al., 2021). While all these approaches have benefits (Hamdi et al., 2020), the absence of a general understanding of how climate change affects urban areas stems from the lack of a climate-consistent, coupled, global high-resolution perspective. *Climate-consistent* here means that all urban areas should be studied under a global and physically plausible atmospheric state across short and long timescales; by *coupled*, we mean that such a perspective considers the feedbacks between terrestrial surfaces and the atmosphere; and *global high-resolution* simulations enable a local perspective on climate impacts anywhere in the world without further postprocessing or limited-area climate downscaling.

Over the past 5 years a community effort was undertaken to realize the first multi-decadal global coupled km-scale simulations (i.e., grid-spacings between 1 and 10 km), facilitated by the increase in computational power and the adaptation of models for efficient performance in such HPCs (Segura et al., 2025). Compared to previous

Methodology: Xabier Pedruzo-Bagazgoitia, Birgit Sützl, Emanuel Dutra
Resources: Xabier Pedruzo-Bagazgoitia, Birgit Sützl, Emanuel Dutra
Supervision: Xabier Pedruzo-Bagazgoitia, Birgit Sützl, Christoph Rüdiger
Validation: Xabier Pedruzo-Bagazgoitia, Birgit Sützl, Emanuel Dutra
Visualization: Xabier Pedruzo-Bagazgoitia, Birgit Sützl
Writing – original draft: Xabier Pedruzo-Bagazgoitia, Birgit Sützl, Emanuel Dutra, Joe McNorton
Writing – review & editing: Xabier Pedruzo-Bagazgoitia, Birgit Sützl, Emanuel Dutra, Joe McNorton, Aristofanis Tsiringakis, Christoph Rüdiger

climate simulations, these km-scale simulations explicitly resolve more of the surface and atmospheric processes driving the climate, such as convection (Becker et al., 2021; Prein et al., 2020) and its impact on surface radiation (Pedruzo-Bagazgoitia et al., 2019) or orography and its impact on large scale circulation and atmospheric blockings (Sandu et al., 2019; Woollings et al., 2018). In addition, these simulations provide local surface granularity with global coverage. These features present a clear opportunity for global impact studies of which, provided an urban parametrization is included, km-scale urban climate analysis is one example that has not been attempted to this day (Rackow et al., 2025). Such analyses could aid climate adaptation and mitigation strategies globally at different governance levels in aspects such as health (Le Roy et al., 2024), energy and infrastructure demands (Nik et al., 2020; Ren & McGregor, 2021), and hazard preparedness (IPCC, 2023a).

For the first time, we leverage global km-scale climate simulations for a systematic urban climate analysis. Here, we (a) develop a generic method to define urban areas and their rural counterparts worldwide, (b) validate over 400 cities globally against satellite land surface temperatures (LST) at 28, 9, and 4.4 km model resolution, and (c) analyze urban climates in multi-decadal km-scale simulations and explore clustering techniques to generalize our findings beyond city-specific conclusions.

2. Cities in Global Coupled km-Scale Climate Simulations

Here, we analyze some of the first ever multi-year global km-scale simulations and validate their performance over urban areas, with a focus on the spatial resolution dependence.

2.1. Simulations

The simulations analyzed in this study were produced during the nextGEMS project cycle 3 (Rackow et al., 2025) and cycle 4 (production cycle, Segura et al., 2025) and use the Integrated Forecasting System (IFS) coupled to the ocean models Nucleus for European Modelling of the Ocean (NEMO 3.4) (Gurvan et al., 2013; Mogensen et al., 2012) or Finite-Element/volumE Sea ice-Ocean Model (FESOM) (Rackow et al., 2023, 2025; Scholz et al., 2019). The IFS (ECMWF, 2024a, 2024b) is a surface-atmosphere coupled model developed and maintained at ECMWF together with its member states. Of particular interest is the urban scheme (McNorton et al., 2021, 2023) present in the IFS land-surface model ecLand (Boussetta et al., 2021). The urban scheme uses a canyon representation and explicitly accounts for radiative trapping, shadowing, and heat storage within the canyon, shaping the diurnal evolution of urban surface temperatures and allowing the simulations to capture the surface urban heat island (SUHI) in a physically consistent way across diverse city types. The urban surface as part of the land-surface model is coupled to the atmosphere via surface fluxes of momentum, heat, and moisture, receiving input from the regional weather and simultaneously impacting it. The model therefore captures interactions between cities and meteorological processes, for example, there is a direct impact on near-surface air temperature, but also humidity (affecting thermal comfort in cities) and city-scale effects such as modified boundary layers. Urban parameters such as height-to-width and road-to-building ratios, emissivities, or heat capacities are spatially homogeneous in the current model version given the lack of model-tested consistent information for cities worldwide (McNorton et al., 2023).

Three ocean-coupled simulations from nextGEMS cycle 3 (Koldunov et al., 2023) are used in Section 2.3 for a global validation of modeled urban surface temperatures. The simulations span 5 consecutive years with horizontal model resolutions of 28, 9, and 4.4 km (hereafter called 4 km) for atmosphere and land producing what is considered a "perpetual 2020": they are initialized on 20 January 2020 and apply the same 2020 greenhouse gas concentrations and aerosol forcings across the entire period (Koldunov et al., 2023; Rackow et al., 2025).

The two 30-year simulations used in Section 3 are the so-called IFS-FESOM production simulations in nextGEMS (Segura et al., 2025; Wieners et al., 2024). These simulations were produced by running the surface-atmosphere model components of IFS at 9 km resolution coupled to the FESOM ocean model at 5 km resolution. The historical simulation is initialized on 1 January 1990 and covers the 1990–2020 period. The future scenario is an analogous simulation initialized using the ECMWF analysis of 20 January 2020 for atmosphere and land, and an ocean span-up over 5 years. Such simulated projection covers the 2020–2050 period and follows the Shared Socioeconomic Pathways scenario SSP3-7.0 (O'Neill et al., 2016) for greenhouse-gas and ozone concentrations. The land-cover information remains constant for all simulations. To our knowledge, the scenario simulation was the first global coupled km-scale and multi-decadal simulation ever completed.

10.1029/2025GL120583

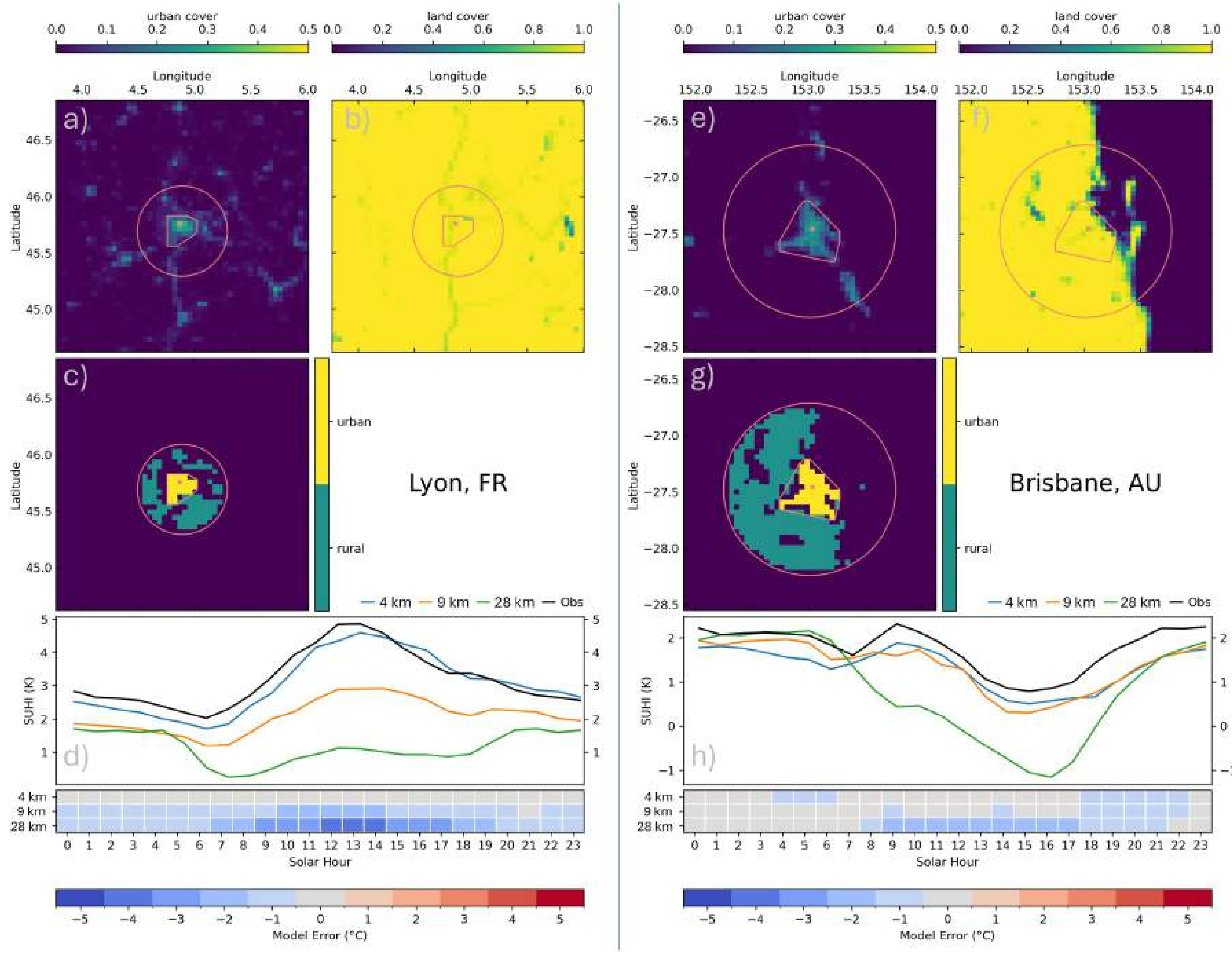

Figure 1. Methodology to define urban and rural agglomerations for Lyon, France (left), and Brisbane, Australia (right) at a resolution of 0.045° with (a/e) urban cover, (b/f) land cover, and (c/g) resulting agglomerations. The red markers indicate the respective city's center reference coordinates; the red outlines show the urban convex hulls (enclosing the urban agglomeration) and the red circles indicate the radius of the rural agglomerations. The summer (JJA for Lyon and DJF for Brisbane) 5-year mean diurnal cycle of the surface urban heat island (SUHI) is shown (d/h) for observations and three different resolutions. Below each diurnal cycle, the heatmaps illustrate the SUHI error made at each hour of the day.

2.2. Defining Urban Agglomerations and Rural Reference Regions

To systematically study cities in global simulations, we developed a methodology to define urban agglomerations and their representative surrounding rural regions based on the cities' center coordinates and the surface cover information used as model input data.

Starting from the center coordinates of a city (e.g., from a global database, see Section 2.3 below), we define the urban agglomeration as the continuous cluster of grid points where urban cover exceeds 10% around the given coordinates (Figures 1a and 1e). The respective surrounding rural agglomeration contains a subset of land grid points within a specified radius from the urban center point. Here, those grid points are defined as land points around the urban agglomeration where the total land cover fraction is larger than 99% (Figures 1b and 1f) and the urban cover is lower than 3%, hence excluding any water or peri-urban regions for a clean rural reference.

Figure 1 illustrates the methodology for the cities of Lyon, France and Brisbane, Australia. The radius defining the rural agglomeration is defined as 1.5 times the mean city width, which is derived from the perimeter of the convex hull enclosing the urban agglomeration (white outlines in Figures 1a–1c and 1e–1g). The scaling factor of 1.5 guarantees a balance between the number of rural and urban points (see Figure S1 in Supporting Information S1).

The urban convex hull may encompass non-urban regions that are embedded by the urban agglomeration (cf. Sützl et al., 2021); and which subsequently are excluded as they are likely directly influenced by the city and could perturb the rural reference values. Figures 1c and 1g show the urban and rural agglomerations determined with this method.

2.3. Critical Role of Resolution for Urban Representation in Models and Satellite Retrievals

Before analyzing the 30-year production simulations, a global validation of the surface urban heat island (SUHI, the difference between area-averaged urban and rural surface temperatures for a given city) was performed to build confidence in the simulations' ability to reproduce realistic urban climates. The IFS surface model ecLand, including the urban scheme, used in the nextGEMS simulations has been running operationally at ECMWF in IFS CY49R1 since November 2024 and has undergone strict development, testing, and validation processes before its operationalization. The validation presented here is an additional test to confirm that the features previously studied at timescales of days and weeks are preserved at multi-annual timescales. The validation uses LST due to its observational global coverage, unlike for other variables like 2-m temperature Hamdi et al. (2020).

This validation uses the Copernicus Land Monitoring Service (CLMS) LST version 3 data set (Copernicus Land Monitoring Service (CLMS), 2026) as a reference. The CLMS product provides global hourly LST on a regular grid with a resolution of about 0.045°, derived from measurements collected onboard the Himawari-8/9, GOES-16, and MSG satellites, the latter operating the 0° and Indian Ocean Data Coverage missions. The LST retrieval is based on a generalized split-window algorithm, using measurements from two adjacent channels within the infrared atmospheric window of each sensor. The LST product is a directional estimate and may not correspond exactly to the integrated skin temperature of a heterogenous urban surface as simulated by the model. However, LST retrievals from geostationary satellites have been successfully used in previous urban studies (e.g., Hurduc et al., 2024; Nogueira et al., 2022). The purpose of using this LST data set is not to resolve or characterize urban signals in detail, but rather to provide an independent observational reference for assessing the realism of the model simulations. The selected LST product has a horizontal resolution close to that of the highest-resolution climate simulations, and is unique in offering near-global coverage and sub-daily (hourly) temporal resolution, enabling a comprehensive evaluation of the diurnal cycle.

To automatically select the cities for validation, we assembled a database with the 10 largest cities per country with a minimum of 100,000 inhabitants using open-source software (joelacus/world-cities). This resulted in a list of 404 cities to validate on the observation reference grid of 0.045° using the methodology described in Section 2.2 (see the list of validated cities in Supporting Information S1).

We analyzed the 5-year mean diurnal cycles of SUHIs for the boreal summer seasons (June, July, August [JJA]) of the Northern Hemisphere (NH) extra-tropics, and austral summer season (December, January, February [DJF]) of the Southern Hemisphere (SH) extra-tropics. In addition, cities within the tropics were assessed for their respective dry seasons (DJF for NH tropics and JJA for SH tropics). Hours with cloud cover above 0.3 were filtered out at gridpoint level due to the lack of analogous observations. We compared the 5-year 2020 control simulations to the observed 2018–2022 period. Focusing on the mean summer/dry-season SUHIs removes varying atmospheric conditions and isolates urban effects over the period when the coupled effects between the urban surface and the atmosphere are the largest.

Figures 1d and 1h shows two examples of the observed and modeled mean diurnal cycles of summer SUHI and the associated model bias for the three resolutions 4, 9, and 28 km. For the medium-sized inland city of Lyon (France), the error reduces gradually with increasing resolution: 4.4 km outperforms the coarser 9 km simulation, while the 28 km simulation hardly shows any urban signal in the diurnal cycle. For the coastal city of Brisbane (Australia), both the 9 and 4 km simulations reproduce the SUHI diurnal variations similarly. Meanwhile, the 28 km simulation struggles to reproduce the diurnal cycle and its correct amplitude. The results for both cities show that the km-scale simulations capture canonical inland SUHI cycles (Lyon) as well as more complex coastal patterns (Brisbane), reflecting the diversity of urban thermal behaviors across different settings. The limited improvement at 4 km compared to 9 km for Brisbane exemplifies that resolution alone does not warrant an improvement: coarse or low quality surface information, missing urban processes in the model or dominance of larger scale factors, especially for coastal or orographically complex cities, are potential contributors. Likely, smaller and medium-sized cities benefit most from a resolution increase from 9 to 4 km, given their limited spatial extent.

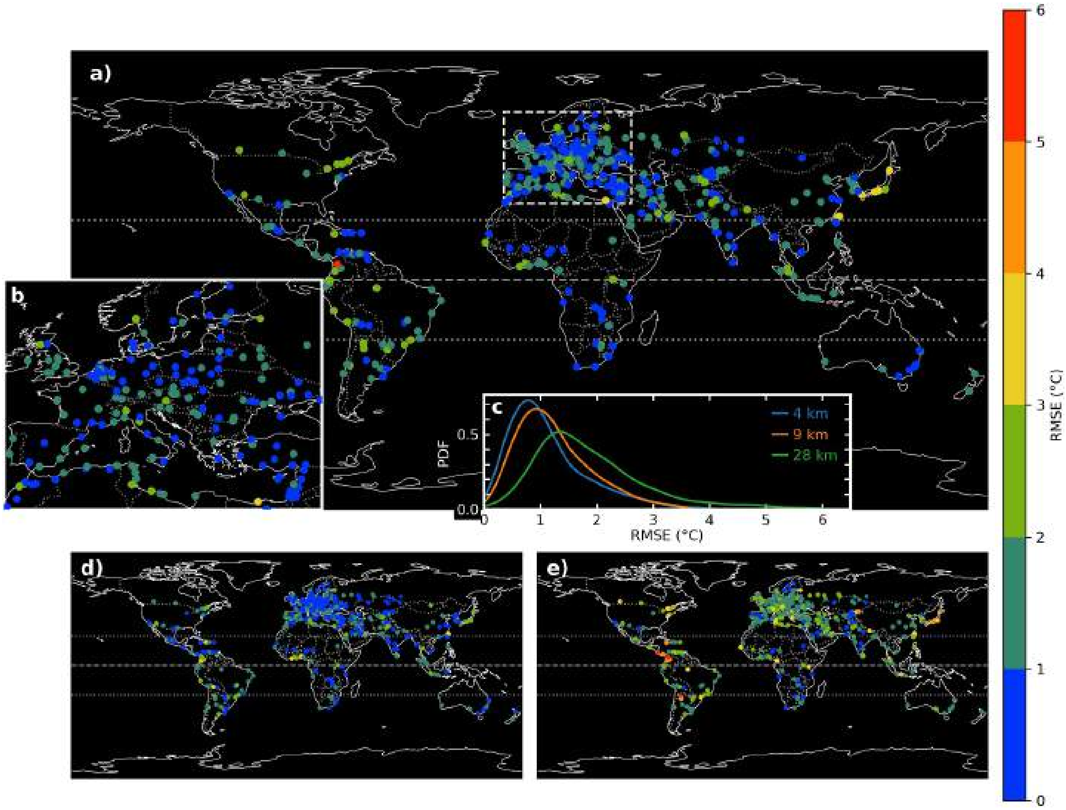

Figure 2. Spatial map of root mean squared error (RMSE) of the mean surface urban heat island diurnal cycle for summer/dry-season for the 404 cities validated in (a) 9 km including (b) a zoom over Europe, (d) 4 km, and (e) 28 km simulations against observations. Dotted and dashed lines indicate the tropics and equator, respectively. The RMSE distribution for the three resolutions is shown in panel (c).

For a global evaluation of model performance and assessment of spatial resolution effects, we computed the root-mean square error (RMSE) of the SUHI mean diurnal cycles over the summer/dry seasons contained in the 5 simulated years for each simulation for the 404 cities. Figures 2a and 2c show that these average daily errors (RMSE values) in the 9 km simulation are overall below 3°C. Errors are smallest in the extratropical regions, albeit slightly larger in the Japanese archipelago. These results demonstrate the robustness of the method for detecting urban areas and their rural counterparts, as well as the reliability of the coupled simulations. For the analysis in Section 3, we applied an RMSE threshold of 4°C to exclude cities where the model performance was particularly poor, which resulted in the removal of Medellín (Colombia). In contrast, the 28 km simulation shows larger RMSE values (Figures 2c and 2e) for most regions compared to 9 km, while 4 km shows improvements particularly for cities in Europe and Eastern Asia that have RMSE above 1°C at 9 km, which may come from better resolving their spatial extent at higher resolution, as shown for Lyon. Despite sporadic increases in RMSE at 4 km compared to 9 km, the RMSE distribution function (Figure 2c) demonstrates a general improvement at 4 km compared to 9 km, and further shows the clear improvement from 28 to 9 km. Supporting Information S1 provides the hourly bias of 4, 9, and 28 km for the SUHI mean diurnal cycle for the 404 cities.

3. Urban Climate Trends

After the previous section confirming realistic SUHIs at km-scale resolution and multi-annual timescales, on top of the validation by McNorton et al. (2021, 2023), this section explores the historical and scenario simulations. These simulations total 60 years of global hourly 9-km simulated resolution data for past, present, and future scenario. The methodology introduced in Section 2.2 identifies around 200 cities at 9 km model resolution that are analyzed below. Note that in this section we focus on 2-m temperature and urban heat island (UHI, 2-m temperature difference) rather than LST and SUHI, as the formers are more relevant metrics for climate analysis.

10.1029/2025GL120583

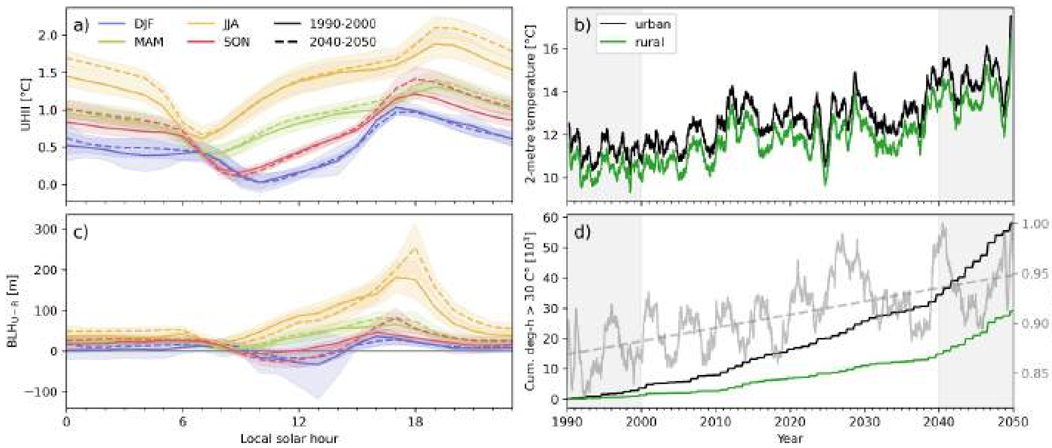

Figure 3. Example diagnostics for Lyon: season-mean diurnal cycles for (a) urban heat island intensity (UHII) and (c) urban-rural boundary layer height difference for the first decade 1990–2000 of the historical simulation (full) and last decade 2040–2050 of the future-scenario simulation (dashed) (see shaded areas in panels (b, d)), respectively, with inter-annual standard deviation in shaded colors; 60-year hourly timeseries of (b) 2-m temperature 1-year rolling-mean for urban (black) and rural (green) areas and (d) urban-rural difference (UHII) (gray) with its long-term trend (linear regression dashed); cumulative degree-hour above 30°C for urban and rural areas (also in panel (d)).

Figure 3 showcases the extensive amount of data available for individual cities. The urban heat island intensity (UHII) in Lyon (Figure 3a) is strongest in summer as expected, and its diurnal variation increases between the 1990–2000 and 2040–2050 decades, particularly in summer and autumn evenings and night-time. The change in UHII stems from the unequal long-term warming of urban and rural areas (Figure 3b) leading to an increase of UHII over time (Figure 3d). Urban surface processes impact the boundary layer above in distinct ways: increased net-radiation due to lower urban surface albedo combined with lower surface evaporation leads to higher surface sensible heat fluxes deepening the boundary layer over urban areas (Oke, 2002). This is visible for most seasons and hours in Lyon, but especially in summer and autumn evenings (Figure 3c). Interestingly, and probably led by future larger UHIIs (Figure 3a), the urban-rural boundary-layer height difference is expected to increase further in the future, potentially impacting near-surface air quality as a consequence of surface-driven increased turbulent mixing within the boundary layer. The available high spatio-temporal data allows to analyze long-term hourly trends in rural and urban areas (Figure 3b), and to compute metrics such as cumulative degree hours above a given threshold (30 here), which is a relevant metric for urban studies (X. Yang et al., 2017) and its impact on health (Jung et al., 2020). Figure 3d shows how the accumulation differs for Lyon's urban and rural areas and how both trends accelerate, albeit stronger for the urban area, after 2040.

To investigate the general impact of climate change and considering the uncertainty of single-model realizations and city peculiarities, we classified cities into distinct groups and analyzed their averaged behavior. We explored clustering along several parameters such as water access, city size, or elevation, but will focus here on results clustered according to four main Köppen-Geiger climate zones based on high-resolution, observation-based climatologies from 1991 to 2020 (Beck et al., 2023): cold, arid, temperate, and tropical. Note that a single city in our data set was categorized as polar, which we added to the cold-cities category.

Figure 4a reveals that temperate cities have the largest UHI intensities at any time of the day, followed by tropical cities; while the largest diurnal UHII variability occurs for arid cities. More interestingly, we find that, unlike for Lyon, UHII decreases under future climate for all cluster averages except for cold climates. The general UHII decrease is explained by a stronger warming of the rural surroundings than the urban area (cf. Figure 4b), which was also concluded by Oleson et al. (2011) and Oleson (2012) at much coarser resolutions, but disagrees with the reported stronger surface warming as observed remotely (Liu et al., 2022). The evolution of mean 2-m temperatures in past and future climates (Figure 4b) shows the strongest warming for cold cities (cf. increase along *x*-axis in Figure 4b), consistent with mountains and high latitudes warming faster in recent (Pepin et al., 2022; Rantanen et al., 2022) and future climate (IPCC, 2023b; Ma et al., 2022). In contrast, tropical cities experience the weakest warming, but the largest increase in tropical nights (cf. increase along *y*-axis in Figure 4b). Average night-time temperatures are already high in the tropics; therefore, small temperature increases are sufficient to re-

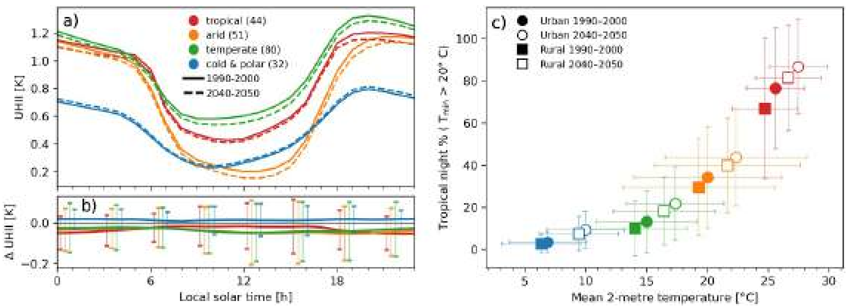

Figure 4. Cluster-mean (a) change in urban heat island intensity (UHII) between the first decade 1990–2000 of the historical simulation (solid) and last decade 2040–2050 of the future-scenario simulation (dashed), cluster mean (b) UHII difference between the shown decades with error bars indicating inter-city standard deviation, and (c) 2-m temperature (x-axis) and percentage of tropical nights (y-axis) for urban (circles) and rural (squares) between 1990–2000 (full) and 2040–2050 (outline) decades. The legend provides the number of cities per cluster.

classify many nights as tropical. Finally, Figure 4b shows that the temperature increase due to climate change is larger than the difference in temperature between urban and rural for all city clusters. The inter-city variability (errorbars in Figures 4b and 4c) suggests that further cluster refinement may decrease result uncertainty.

4. Conclusions and Outlook

For the first time there are global, km-scale, urban-aware simulations of past and future climates that permit the analysis of hundreds of cities and their interactions with other Earth System components, opening unprecedented possibilities to study urban climate change. We propose here a method to systematically extract data of urban agglomerations and their respective rural surroundings, and validate it in combination with km-scale, multi-year, global simulations employing three different spatial resolutions for over 400 cities worldwide. Results confirmed that the simulations generally capture urban-rural thermal contrasts and that the method to define urban and rural agglomerations is sufficiently general to do so; further it is shown that km-scale resolutions, for example, of 9 km or finer, are necessary to reliably represent these thermal effects. This requirement is likely due to most cities not being large enough (or having a sufficiently high urban fraction) to induce these thermal effects at coarser resolutions. The results further show that the simulations successfully represent urban-driven atmospheric impacts, such as distinct urban boundary layer heights.

A caveat of global multidecadal km-scale climate simulations is the limited number available due to their computational cost. Their scarcity presents a challenge to address the uncertainties of input data (e.g., reliability, change with urbanization), future scenarios, or local model biases, to name a few examples. In order to address some of these aspects, but also to quantify generalized effects of cities under climate change, we clustered cities of similar characteristics to compute a "city-ensemble." After exploring several criteria, clustering was done by climate zones as it provided the most distinct clusters.

Additional assessments of result uncertainty could involve comparisons with alternative approaches for delineating urban and rural areas (Q. Yang et al., 2024) and adding to the simulations realistic time-varying surface properties, including non-homogeneous urban properties, consistent with the historical record and scenarios. Future work should incorporate spatially varying urban properties given recently developed km-scale global data sets Cheng et al. (2025). For example, McNorton et al. (2023) found that the assumption of homogeneous building-to-road ratio results in model biases, affecting the simulation of winds at airports in particular, since such ratios do not apply to road-dominated environments.

This analysis suggests that on average rural areas experience a stronger warming with climate change than urban areas, which may decrease future UHI effects for cities in most climate zones; and while this decrease of UHII is not the case for average cold cities, these cities will experience the strongest temperature increases in the simulated scenario. A rural drying, or an "aridification" as also suggested by Oleson (2012) on coarser simulations may be a driver for the stronger warming in rural areas, however this effect deserves further analysis.

This study primarily presents information on near-surface temperature contained in km-scale climate simulations. However, the data contained therein allows to investigate a myriad of processes and scientific questions: humidity effects in urban areas linking to thermal comfort, the prevalence of the so-called urban wind island (Droste et al., 2018), interactions between urban areas and the atmospheric boundary layer at both short and long timescales, the potential triggering of convection and downwind precipitation due to urban properties (Sui et al., 2024), among others. The km-scale character allows for city-specific analysis for those interested, while the global coverage permits urban research beyond a few well-studied cities (Montfort et al., 2025). Most importantly, these simulations allow to address these questions combined with the impact of climate change.

We believe the urban community can benefit from adding coupled km-scale climate simulations to their repertoire, and that the climate community has now the chance to study urban phenomena missing in the field to this date. Projects aiming to further develop global km-scale climate models and their understanding such as EERIE, WARMWORLD or TERRA DT, will continue to produce improved multi-decadal simulations in the years to come, opening an opportunity to address uncertainty with a model-ensemble approach. In parallel, plans for a third intercomparison of km-scale global models are on-going, with a 1-year targeted simulation time (Takasuka et al., 2024). The Destination Earth initiative, funded by the European Commission, is already operationalizing the production of such simulations in the context of the Climate Adaptation Digital Twin (Doblas-Reyes et al., 2026). In Destination Earth, 3 km-scale coupled climate models are continuously producing multi-decadal simulations at 5 km resolution available on the Destin Eplatform for European public and selected partners worldwide.

Conflict of Interest

The authors declare no conflicts of interest relevant to this study.

Availability Statement

The analyzed nextGEMS simulations are openly accessible and archived in the World Data Center for Climate at https://doi.org/10.26050/WDCC/nextGEMS3 (Koldunov et al., 2023) and https://doi.org/10.35095/WDCC/nextGEMS_addinfov1 (Wieners et al., 2024). In addition, the historical and scenario simulations are available via the EERIE cloud hosted by DKRZ and at the Destination Earth Data Lake. The scripts and notebooks used to perform the analysis presented here can be found in Pedruzo-Bagazgoitia and Sützl (2026).

Acknowledgments

We thank João Martins, Sebastian Milinski, and Thomas Rackow for helpful discussions, and Chiel van Heerwaarden for support in using Köppen-Geiger climate zones. We would also like to thank two anonymous reviewer for providing insightful comments on the first version of the manuscript. This research was supported by the Horizon 2020 project nextGEMS (Grant 101003470) and the Destination Earth programme funded by the European Commission and implemented by ECMWF, ESA, and EUMETSAT. The analysis and analyzed simulations were performed on Deutsches Klimarechenzentrum (DKRZ) facilities under Projects bm1235 and bb1153.

References

Beck, H. E., McVicar, T. R., Vergopolan, N., Berg, A., Lutsko, N. J., Dufour, A., et al. (2023). High-resolution (1 km) Köppen-Geiger maps for 1901–2099 based on constrained CMIP6 projections. *Scientific Data*, *10*(1), 724. https://doi.org/10.1038/s41597-023-02549-6

Becker, T., Bechtold, P., & Sandu, I. (2021). Characteristics of convective precipitation over tropical Africa in storm-resolving global simulations. *Quarterly Journal of the Royal Meteorological Society*, *147*(741), 4388–4407. https://doi.org/10.1002/qj.4185

Boussetta, S., Balsamo, G., Arduini, G., Dutra, E., McNorton, J., Choulga, M., et al. (2021). ECLAND: The ECMWF land surface modelling system. *Atmosphere*, *12*(6), 723. https://doi.org/10.3390/atmos12060723

Cheng, Y., Zhao, L., Chakraborty, T., Oleson, K., Demuzere, M., Liu, X., et al. (2025). U-surf: A global 1 km spatially continuous urban surface property dataset for kilometer-scale urban-resolving Earth system modeling. *Earth System Science Data*, *17*(5), 2147–2174. https://doi.org/10.5194/essd-17-2147-2025

Copernicus Land Monitoring Service (CLMS). (2026). Land surface temperature 2018-present (raster 3 km), global, hourly—Version 3. https://doi.org/10.2909/3911012ec6a-a073-4cb5-95f4-95dad6f4f423

Doblas-Reyes, F. J., Kontkanen, J., Sandu, I., Acosta, M., Al Turjmam, M. H., Alsina-Ferrer, I., et al. (2026). The destination Earth digital twin for climate change adaptation. *Geoscientific Model Development*, *19*(7), 2821–2848. https://doi.org/10.5194/gmd-19-2821-2026

Droste, A. M., Steeneveld, G. J., & Holtslag, A. A. M. (2018). Introducing the urban wind island effect. *Environmental Research Letters*, *13*(9), 094007. https://doi.org/10.1088/1748-9326/aad8ef

Duchêne, F., Schaeybroeck, B. V., Caluwaerts, S., Troch, R. D., Hamdi, R., & Termonia, P. (2020). A statistical–dynamical methodology to downscale regional climate projections to urban scale. *Journal of Applied Meteorology and Climatology*, *59*(6), 1109–1123. https://doi.org/10.1175/JAMC-D-19-0104.1

ECMWF. (2024a). IFS documentation Cy49r1 - Part iii: Dynamics and numerical procedures. In *(chap. 3)*. https://doi.org/10.21957/d04fb7a27e

ECMWF. (2024b). IFS documentation Cy49r1 - Part iv: Physical processes. In *(chap. 4)*. https://doi.org/10.21957/c731ee1102

Gurvan, M., Bourdallé-Badie, R., Bouttier, P.-A., Bricaud, C., Bruciaferri, D., Calvert, D., et al. (2013). Nemo ocean engine. *Zenodo*. https://doi.org/10.5281/zenodo.1475234

Hamdi, R., Kusaka, H., Doan, Q.-V., Cai, P., He, H., Luo, G., et al. (2020). The state-of-the-art of urban climate change modeling and observations. *Earth Systems and Environment*, *4*(4), 631–646. https://doi.org/10.1007/s41748-020-00193-3

Hurduc, A., Ermida, S. L., & DaCamara, C. C. (2024). On the suitability of different satellite land surface temperature products to study surface urban heat islands. *Remote Sensing*, *16*(20), 3765. https://doi.org/10.3390/rs16203765

IPCC. (2023a). Cities, settlements and key infrastructure. In *Climate change 2022 – Impacts, adaptation and vulnerability: Working group ii contribution to the sixth assessment report of the intergovernmental panel on climate change* (pp. 907–1040). Cambridge University Press.

IPCC. (2023b). Future global climate: Scenario-based projections and near-term information. In *Climate change 2021 – The physical science basis: Working group i contribution to the sixth assessment report of the intergovernmental panel on climate change* (pp. 553–672). Cambridge University Press.

Johannsen, F., Soares, P. M., & Langendijk, G. S. (2024). On the deep learning approach for improving the representation of urban climate: The Paris urban heat island and temperature extremes. *Urban Climate*, *56*, 102039. https://doi.org/10.1016/j.uclim.2024.102039

Jung, C.-C., Hsia, Y.-F., Hsu, N.-Y., Wang, Y.-C., & Su, H.-J. (2020). Cumulative effect of indoor temperature on cardiovascular disease–related emergency department visits among older adults in Taiwan. *Science of the Total Environment*, *731*, 138958. https://doi.org/10.1016/j.scitotenv.2020.138958

Koldunov, N., Kölling, T., Pedruzo-Bagazgoitia, X., Rackow, T., Redler, R., Sidorenko, D., et al. (2023). *nextGEMS: Output of the model development cycle 3 simulations for icon and IFS*. World Data Center for Climate (WDCC) at DKRZ. https://doi.org/10.26050/WDCC/nextGEMS_cyc3

Langendijk, G. S., Halenka, T., Hoffmann, P., Adinolfi, M., Aldama Campino, A., Asselin, O., et al. (2024). Towards better understanding the urban environment and its interactions with regional climate change - The WCRP CORDEX flagship pilot study URB-RCC. *Urban Climate*, *58*, 102165. https://doi.org/10.1016/j.uclim.2024.102165

Lauwaet, D., Hooyberghs, H., Maiheu, B., Lefebvre, W., Driesen, G., Van Looy, S., & De Ridder, K. (2015). Detailed urban heat island projections for cities worldwide: Dynamical downscaling CMIP5 global climate models. *Climate*, *3*(2), 391–415. https://doi.org/10.3390/cli3020391

Lemonsu, A., Kounkou-Arnaud, R., Desplat, J., Salagnac, J.-L., & Masson, V. (2013). Evolution of the Parisian urban climate under a global changing climate. *Climatic Change*, *116*(3), 679–692. https://doi.org/10.1007/s10584-012-0521-6

Le Roy, B., Dixon, K. W., & Adams-Smith, D. (2024). High-resolution urban climate simulations for heat and health applications in Philadelphia. *Urban Climate*, *57*, 102114. https://doi.org/10.1016/j.uclim.2024.102114

Liu, Z., Zhan, W., Bechtel, B., Voogt, J., Lai, J., Chakraborty, T., et al. (2022). Surface warming in global cities is substantially more rapid than in rural background areas. *Communications Earth & Environment*, *3*(1), 219. https://doi.org/10.1038/s43247-022-00539-x

Ma, N., Jiang, J. H., Hou, K., Lin, Y., Vu, T., Rosen, P. E., et al. (2022). 21st century global and regional surface temperature projections. *Earth and Space Science*, *9*(12), e2022EA002662. https://doi.org/10.1029/2022EA002662

McNorton, J., Agustí-Panareda, A., Arduini, G., Balsamo, G., Bousserez, N., Boussetta, S., et al. (2023). An urban scheme for the ECMWF integrated forecasting system: Global forecasts and residential CO_2 emissions. *Journal of Advances in Modeling Earth Systems*, *15*(3), e2022MS003286. https://doi.org/10.1029/2022ms003286

McNorton, J., Arduini, G., Bousserez, N., Agustí-Panareda, A., Balsamo, G., Boussetta, S., et al. (2021). An urban scheme for the ECMWF integrated forecasting system: Single-column and global offline application. *Journal of Advances in Modeling Earth Systems*, *13*(6), e2020MS002375. https://doi.org/10.1029/2020ms002375

Mogensen, K., Keeley, S., & Towers, P. (2012). *Coupling of the nemo and ifs models in a single executable (No. 673)*. ECMWF. https://doi.org/10.21957/rfplwzuol

Montfort, S., Callaghan, M., Creutzig, F., Lamb, W. F., Lu, C., Repke, T., et al. (2025). Systematic global stocktake of over 50,000 urban climate change studies. *Nature Cities*, *2*(7), 613–625. https://doi.org/10.1038/s44284-025-00260-8

Nik, V. M., Perera, A. T. D., & Chen, D. (2020). Towards climate resilient urban energy systems: A review. *National Science Review*, *8*(3), nwaa134. https://doi.org/10.1093/nsr/nwaa134

Nogueira, M., Hurduc, A., Ermida, S., Lima, D. C. A., Soares, P. M. M., Johannsen, F., & Dutra, E. (2022). Assessment of the paris urban heat island in ERA5 and offline SURFEX-TEB (v8.1) simulations using the METEOSAT land surface temperature product. *Geoscientific Model Development*, *15*(14), 5949–5965. https://doi.org/10.5194/gmd-15-5949-2022

Oke, T. R. (2002). *Boundary layer climates*. Routledge.

Oleson, K. W. (2012). Contrasts between urban and rural climate in CCSM4 CMIP5 climate change scenarios. *Journal of Climate*, *25*(5), 1390–1412. https://doi.org/10.1175/JCLI-D-11-00098.1

Oleson, K. W., Bonan, G. B., Feddema, J., & Jackson, T. (2011). An examination of urban heat island characteristics in a global climate model. *International Journal of Climatology*, *31*(12), 1848–1865. https://doi.org/10.1002/joc.2201

O'Neill, B. C., Tebaldi, C., van Vuuren, D. P., Eyring, V., Friedlingstein, P., Hurtt, G., et al. (2016). The scenario model intercomparison project (ScenarioMIP) for CMIP6. *Geoscientific Model Development*, *9*(9), 3461–3482. https://doi.org/10.5194/gmd-9-3461-2016

Pedruzo-Bagazgoitia, X., Jiménez, P. A., Dudhia, J., & de Arellano, J. V.-G. (2019). Shallow cumulus representation and its interaction with radiation and surface at the convection gray zone. *Monthly Weather Review*, *147*(7), 2467–2483. https://doi.org/10.1175/MWR-D-19-0030.1

Pedruzo-Bagazgoitia, X., & Sützl, B. (2026). Scripts for 'unlocking urban climate change analysis in global kilometer-scale climate simulations'. *Zenodo*. https://doi.org/10.5281/zenodo.20414518

Pepin, N. C., Arnone, E., Gobiet, A., Haslinger, K., Kotlarski, S., Notarnicola, C., et al. (2022). Climate changes and their elevational patterns in the mountains of the world. *Reviews of Geophysics*, *60*(1), e2020RG000730. https://doi.org/10.1029/2020RG000730

Prein, A. F., Rasmussen, R., Castro, C. L., Dai, A., & Minder, J. (2020). Special issue: Advances in convection-permitting climate modeling. *Climate Dynamics*, *55*(1), 1–2. https://doi.org/10.1007/s00382-020-05240-3

Rackow, T., Hegewald, J., Koldunov, N. V., Mogensen, K., Scholz, P., Sidorenko, D., & Streffing, J. (2023). FESOM2.5 source code used in nextGEMS cycle 3 simulations with IFS-FESOM. *Zenodo*. https://doi.org/10.5281/zenodo.10225420

Rackow, T., Pedruzo-Bagazgoitia, X., Becker, T., Milinski, S., Sandu, I., Aguridan, R., et al. (2025). Multi-year simulations at kilometre scale with the integrated forecasting system coupled to FESOM2.5 and NEMOV3.4. *Geoscientific Model Development*, *18*(1), 33–69. https://doi.org/10.5194/gmd-18-33-2025

Rantanen, M., Karpechko, A. Y., Lipponen, A., Nordling, K., Hyvärinen, O., Ruosteenoja, K., et al. (2022). The arctic has warmed nearly four times faster than the globe since 1979. *Communications Earth & Environment*, *3*(1), 168. https://doi.org/10.1038/s43247-022-00498-3

Ren, C., & McGregor, G. (2021). *Urban climate science for planning healthy cities*. Springer.

Sandu, I., van Niekerk, A., Shepherd, T. G., Vosper, S. B., Zadra, A., Bacmeister, J., et al. (2019). Impacts of orography on large-scale atmospheric circulation. *npj Climate and Atmospheric Science*, *2*(1), 10. https://doi.org/10.1038/s41612-019-0065-9

Scholz, P., Sidorenko, D., Gurses, O., Danilov, S., Koldunov, N., Wang, Q., et al. (2019). Assessment of the finite-volume sea ice-ocean model (FESOM2.0) – Part 1: Description of selected key model elements and comparison to its predecessor version. *Geoscientific Model Development*, *12*(11), 4875–4899. https://doi.org/10.5194/gmd-12-4875-2019

Segura, H., Pedruzo-Bagazgoitia, X., Weiss, P., Müller, S. K., Rackow, T., Lee, J., et al. (2025). nextGEMS: Entering the era of kilometer-scale Earth system modeling. *Geoscientific Model Development*, *18*(20), 7735–7761. https://doi.org/10.5194/gmd-18-7735-2025

Sui, X., Yang, Z.-L., Shepherd, M., & Niyogi, D. (2024). Global scale assessment of urban precipitation anomalies. *Proceedings of the National Academy of Sciences of the United States of America*, *121*(38), e2311496121. https://doi.org/10.1073/pnas.2311496121

Sützl, B. S., Rooney, G. G., Finnenkoetter, A., Bohnenstengel, S. I., Grimmond, S., & van Reeuwijk, M. (2021). Distributed urban drag parametrization for sub-kilometre scale numerical weather prediction. *Quarterly Journal of the Royal Meteorological Society*, *147*(741), 3940–3956. https://doi.org/10.1002/qj.4162

Takasuka, D., Satoh, M., Miyakawa, T., Kodama, C., Klocke, D., Stevens, B., et al. (2024). A protocol and analysis of year-long simulations of global storm-resolving models and beyond. *Progress in Earth and Planetary Science*, *11*(1), 66. https://doi.org/10.1186/s40645-024-00668-1

Wieners, K.-H., Rackow, T., Aguridan, R., Becker, T., Beyer, S., Cheedela, S. K., et al. (2024). *nextGEMS: Catalogs of full output of the production simulations for icon and IFS*. World Data Center for Climate (WDCC) at DKRZ. https://doi.org/10.35095/WDCC/nextGEMS_prod_addinfov1

Woollings, T., Barriopedro, D., Methven, J., Son, S.-W., Martius, O., Harvey, B., et al. (2018). Blocking and its response to climate change. *Current Climate Change Reports*, *4*(3), 287–300. https://doi.org/10.1007/s40641-018-0108-z

Yang, Q., Xu, Y., Chakraborty, T., Du, M., Hu, T., Zhang, L., et al. (2024). A global urban heat island intensity dataset: Generation, comparison, and analysis. *Remote Sensing of Environment*, *312*, 114343. https://doi.org/10.1016/j.rse.2024.114343

Yang, X., Li, Y., Luo, Z., & Chan, P. W. (2017). The urban cool island phenomenon in a high-rise high-density city and its mechanisms. *International Journal of Climatology*, *37*(2), 890–904. https://doi.org/10.1002/joc.4747

Zhao, L., Lee, X., Smith, R. B., & Oleson, K. (2014). Strong contributions of local background climate to urban heat islands. *Nature*, *511*(7508), 216–219. https://doi.org/10.1038/nature13462

Zhao, L., Oleson, K., Bou-Zeid, E., Krayenhoff, E. S., Bray, A., Zhu, Q., et al. (2021). Global multi-model projections of local urban climates. *Nature Climate Change*, *11*(2), 152–157. https://doi.org/10.1038/s41558-020-00958-8